Research Project in Mechatronics Engineering

Final Research Report

A Modular Robotic Mechanism for Discrete Rock Sample Collection on Mars

Sophia Schulz

Project Report ME001-2024

Co-worker: Rahul Bhati
Supervisor: Dr Minas Liarokapis

13 October 2024

UNIVERSITY OF AUCKLAND
Waipapa Taumata Rau
NEW ZEALAND

ENGINEERING
DEPARTMENT OF MECHANICAL AND MECHATRONICS ENGINEERING

ME001-2024

A Modular Robotic Mechanism for Discrete Rock Sample Collection on Mars

Sophia Schulz

ABSTRACT

The collection of unique geological samples like silica sinter deposits on Mars, which are critical in the search for extraterrestrial life, is currently hindered by the absence of specialized sampling mechanisms designed with these unique rock structures in mind. Robotic systems have emerged as essential tools for exploring extraterrestrial environments as they can operate in conditions that are inhospitable or unreachable by humans, thus reducing costs and risks associated with manned space missions. In the context of Mars exploration, developing robotic systems capable of precisely collecting geological samples like silica sinters is key to advancing the search for signs of past or present life.

This report details the design, construction, and validation of a novel autonomous sampling system engineered to address this gap, offering a solution for collecting and preserving these geolotical features for analysis. The system features a specialized end effector capable of grasping rocks with different morphologies and varying degrees of brokenness, showcasing its versatility in handling a diverse range of samples. The design employs innovative fin-ray-inspired finger structures made from polylactic acid (PLA) and thermoplastic polyurethane (TPU), each selected for their unique properties to enhance the performance of the end effector during the scooping and lifting phases of the sampling process.

Extensive validation testing revealed the end effector's high success rate in grasping larger samples while preserving essential surface features critical for analysis. Comparative analyses demonstrated that PLA fingers excelled during the scooping phase due to their lower friction characteristics, while TPU fingers performed better with broken samples thanks to their flexibility and higher friction that minimized slippage. These findings suggest that a hybrid design, integrating the advantageous features of both materials, could further enhance grasping performance.

Future work will focus on refining the end effector design for seamless integration with the cutting tool, addressing positional error challenges, and investigating methods for stabilizing rocks during sampling. Overall, this project significantly advances the development of tools to collect silica sinter deposits on Mars, which are of great importance in the ongoing search for signs of extraterrestrial life.

DECLARATION

Student

I ……Sophia Schulz…….. hereby declare that:

1. This report is the result of the final year project work carried out by my project partner (see cover page) and I under the guidance of our supervisor (see cover page) in the 2024 academic year at the Department of Mechanical Engineering, Faculty of Engineering, University of Auckland.
2. This report is not the outcome of work done previously.
3. This report is not the outcome of work done in collaboration, except that with a project sponsor as stated in the text.
4. This report is not the same as any report, thesis, conference article or journal paper, or any other publication or unpublished work in any format.

In the case of a continuing project: State clearly what has been developed during the project and what was available from previous year(s):

Signature: _____

Date: 13/10/24

Supervisor

I confirm that the project work undertaken by this student in the 2024 academic year ~~**is**~~ **/ is not** (*strikethrough as appropriate*) part of a continuing project, components of which have been completed previously.

Comments, if any:

Signature: _____

Date: 13/10/2024

Table of Contents

List of Figures

List of Tables

Acknowledgements

Firstly, I want to thank Rahul Bhati for being an amazing project partner, for challenging me at every step and always being willing to help. You're an incredible engineer and it's always a pleasure working with you.

I also want to thank Dr Minas Liarokapis for your guidance and wisdom as our supervisor throughout the year. Thank you for your patience and encouragement during the project.

My gratitude also extends towards Angus Lynch, Sophia Zhang and Emanuele Romano for your time and assistance in the labs with sourcing equipment and offering advice.

Glossary of Terms

Autonomous Sampling Mechanism	A robotic system designed to collect geological samples without human intervention.
End Effector	The part of a robotic arm designed to interact with its environment and perform a specific task.
Positional Error	A misalignment between an end effector (usually a gripper) and the object being interacted with, potentially affecting the success of the task being carried out.
Extraterrestrial Life	Life that originates outside of Earth, a primary focus of Mars exploration missions.
Morphology	Referring to the shape and structure of geological samples.

Abbreviations

3D	3-Dimensional
CAD	Computer Aided Design
DOF	Degrees of Freedom
PLA	Polylactic Acid (referring to 3D-printing filament)
RPM	Revolutions Per Minute
TPU	Thermoplastic Polyurethane (referring to 3D-printing filament)
UAV	Unmanned Aerial Vehicle

1. Introduction

Robotic systems are indispensable in space exploration, advancing scientific discovery while minimizing the risks and costs associated with human missions. Robots eliminate the need for astronaut life support and return trips, making them safer and more cost-effective. Additionally, through lightweight and energy-efficient design, they can perform extended missions across vast distances. The ability of robotic systems to process large amounts of data quickly and execute tasks with high precision makes them particularly suitable for exploring harsh environments on other planets. These features make robotic missions a safer and more efficient alternative to human exploration, where the risks associated with long-term space travel are still significant [1].

The primary motivation for robotic space exploration is to advance knowledge in areas of science and technology and answer profound questions about life's existence in the universe. The search for life beyond Earth is a notable objective, carried out through the study of atmospheric conditions, geological features, and other characteristics on other planets. Rock sampling is key to this effort, particularly on Mars, where geological formations may hold preserved signs of microbial life. However, robotic systems attempting to carry out these sampling efforts must be highly robust to withstand extreme environments, including intense radiation and temperatures. They also require a high degree of autonomy since real-time communication with Earth is limited by vast distances.

Several pioneering missions have demonstrated the capabilities of robotic exploration on Mars. Rovers such as Curiosity [2] and Perseverance [3] have made significant discoveries using scooping mechanisms and coring drills to collect samples from ground level. In addition to ground-based vehicles, UAVs have more recently been the subject of development for Mars exploration, with the Mars Helicopter Ingenuity making history by performing the first vertical-takeoff-and-landing flight on Mars. Ingenuity has demonstrated the potential of aerial systems for accessing geological features that were unreachable by rovers (eg. due to steep hills, cliffs or otherwise challenging terrain) [4], and shows promise for the continued development and use of UAVs on Mars.

Despite the potential of UAVs, significant challenges exist for integrating them with rock collection systems. Unlike ground-based rovers, UAVs have limited payload capacities, battery life, and hovering stability, particularly in Mars' thin atmosphere. The unpredictable wind conditions and reduced gravity on Mars add complexity to the precision required for rock sampling. UAVs must also account for positional errors and uneven terrain during collection, as small deviations can lead to unsuccessful sampling attempts. Consideration for the positioning accuracy and precision of UAV-mounted systems is crucial for ensuring the successful sampling of geological features.

One of the key goals of these missions is collecting geological samples that could reveal signs of life on Mars. Particular rocks of interest include siliceous sinter deposits (or silica sinters), formed near hot springs such as Mars Pool, Rotokawa in the Taupo Volcanic Zone in New Zealand [5]. These Earth deposits contain preserved microbial communities and have similar characteristics to some geological formations on Mars [6]. If sampled, the Mars deposits may offer insights into whether life had existed at one point on the planet. However, these rocks' unique characteristics, including their variability in porosity and hardness, pose significant challenges for robotic sampling systems. No existing mechanism has been designed to autonomously sample these geological features. Thus, there is strong motivation to develop a novel system capable of overcoming these challenges.

This project is driven by the potential for silica sinters on Mars to contain signs of life. Given the planet's distance from Earth, developing an autonomous system to collect these rock samples is critical. The project aims to design, develop, and validate a robotic mechanism for sampling these geological formations, tailored to the specific challenges and needs they pose. Additionally, the consideration of using a UAV platform for this system is desired: such a platform enhances the system's sampling capability by allowing for travel to distant and otherwise unreachable features. The following sections will review relevant literature on the geology of the target rocks and existing sampling concepts. This paper will then discuss the design, development and validation of a prototype sampling system, with particular focus on the end effector design, and overall considerations for system integration with a UAV platform.

1.1 Research Scope and Objectives

The scope of this project is to develop an autonomous, modular sampling mechanism capable of collecting rock samples of varying morphologies. The primary focus is to sample in a manner that preserves the integrity of the rock for subsequent analysis while addressing potential variability in rock properties. Through experimental testing, the project also encompasses the evaluation of the design's performance and limitations in sampling rocks of diverse shapes and structures. This assessment aims to provide valuable insights for future enhancements to optimize the mechanism's effectiveness for sampling in Martian conditions, while also considering feasibility for integration on a UAV platform.

The objectives of this project are as follows:

- Investigate the characteristics and relevant properties of the target rock sample, including the challenges these characteristics pose for sampling efforts,
- Investigate various sampling mechanism design concepts, focusing on innovative approaches that enhance adaptability and reduce weight and complexity,
- Design and develop a sampling mechanism prototype capable of collecting the rock of interest for analysis,
- Assess and validate the performance of the sampling mechanism prototype in executing sampling procedures with rocks of varying morphologies.

2. Related Work

2.1 Literature on Rock of Interest

Hydrothermal silica deposits on Mars resembling terrestrial hot spring structures are prime targets in the search for evidence of extraterrestrial life. These deposits, such as those found by the Spirit Rover in the Columbia Hills of Gusev Crater [6], exhibit textures and mineralogical properties akin to digitate silica structures observed in modern geothermal locations such as El Tatio, Chile, and Rotokawa, New Zealand [5]. The formation of these deposits through minerals evaporating near hot springs allow for the preservation of biosignatures that, if analysed, could point to signs of life on Mars.

Key features for analysis include millimetre-scale surface protrusions known as digitates (Figure 1). Crucially, these digitates must be sampled in one piece due to the need for intact internal textures to properly analyse their depositional history. Additionally, the Mars

deposits are located on the ground and usually over a unit of bedrock [6], meaning that sampling must take place over these ground deposits with a high degree of precision to collect the millimetre-scale features.

Studies of terrestrial digitate silica structures have revealed critical insights into their physical properties, including bulk porosity that varies between 4.7% and 21.3% [5]. These variations in porosity, along with nano-scale density differences, play a significant role in the mechanical strength of geological materials. Specifically, higher porosity correlates with weaker material, affecting the development and propagation of fractures. Successful sampling on Mars thus requires consideration of these material properties of siliceous deposits to ensure effective engagement with rocks of varying and unpredictable hardness and breaking patterns.

Based on discussions with Michael Rowe and Kathleen Campbell, two researchers at the University of Auckland in the Faculty of Science and authors of notable papers in this field including Nersezova et. al. [5], a reasonably sized sample for analysis should contain at least 3 digitates but be lightweight enough for transport off the planet (100 grams maximum). These sampling requirements and rock characteristics will be taken into consideration for the following analysis of previous work conducted in the design of sampling mechanisms.

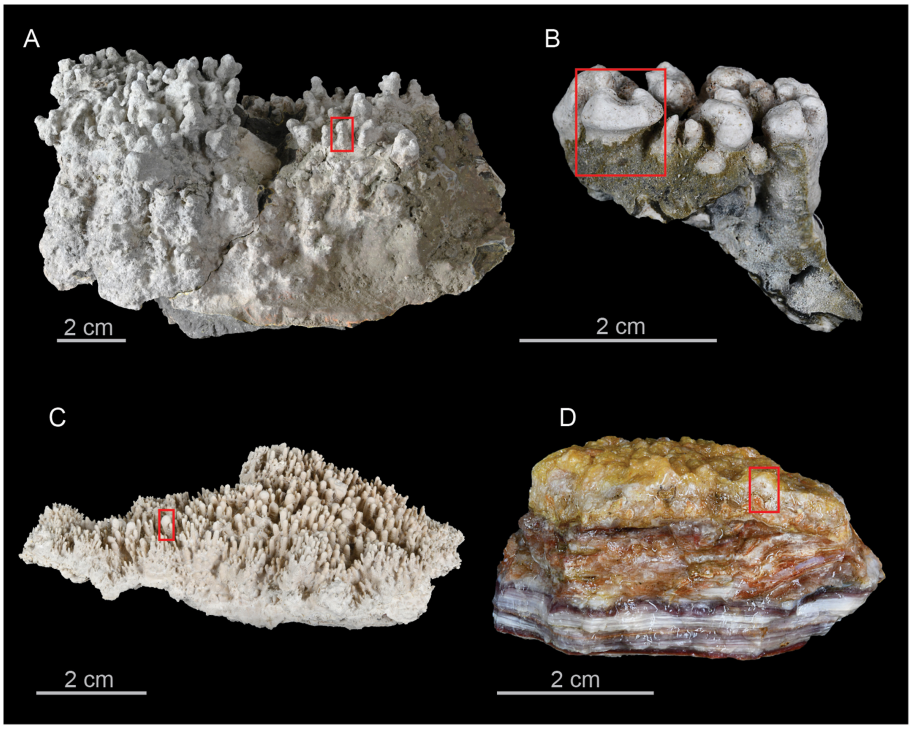

Figure 1 Images of rock samples with digitate features [5].

2.2 Related Work on Autonomous Rock Collection

Literature concerning rock collection includes papers detailing the sampling methods used by the Mars Curiosity and Perseverance Rovers, as well as other experimental designs. Concepts generally focus on either the rock separating method (eg. drilling or scooping) or the rock caching method (eg. gripping or storing), or both. Literature on drilling techniques for mining robots was also reviewed, although the applications and thus the design needs vary significantly. Designs considered here have been primarily created for Unmanned Ground Vehicle (UGV) applications.

Anderson et al. [2] describe the Mars Science Laboratory (MSL) Curiosity Rover's sampling method, which involved collecting granular rock using a scooping mechanism. While this method successfully delivered samples for analysis, it caused material to adhere to the walls of the sampling mechanism, leading to potential sieve clogging and contamination risks. A cleaning method utilizing shock mechanisms, termed thwackers, was introduced to dislodge about 80-90% of adhered material. However, this approach caused excessive stress on some welds, resulting in delamination. Due to these issues, the Curiosity scooping method was not adopted for the Perseverance Rover developed afterwards. Furthermore, the scooping technique was limited to ground-based collection of particles smaller than 150 μm and would not be suitable for larger features such as digitates.

The Perseverance Rover's Sampling and Caching Subsystem (SCS), as outlined by Moeller et al. [3], significantly advanced sample collection capabilities by using a robotic arm and rotary-percussive coring drill. This system allowed the collection of rock cores up to 76 mm in depth and 13 mm in diameter. The robotic arm applied controlled force to the target, stabilizing the coring drill and enabling sampling on surfaces with up to 20 degrees of inclination and height variations of $\pm$ 20 mm. Seals and filters minimized dust interference during drilling, while a second robotic arm with a compliant end-effector handled sample tubes. Although this method provided advantages in preserving stratigraphy and collecting larger samples, the Corer assembly's 23.5 kg weight makes it impractical for UAV integration. An image of the Corer is included below (Figure 2).

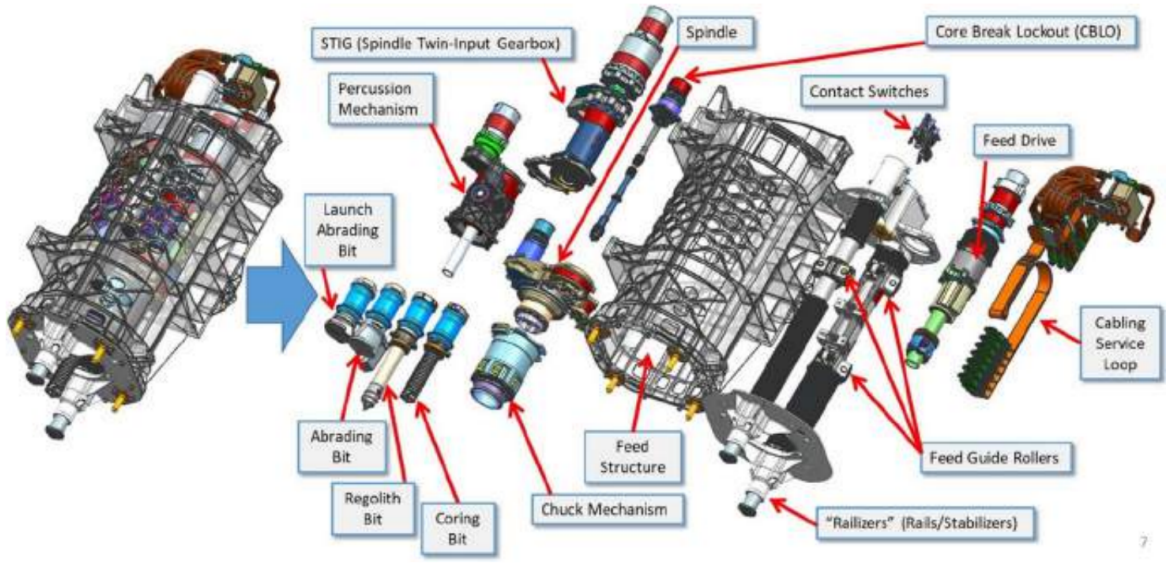

Figure 2 Sampling and Caching Subsystem Corer configuration [3].

Alternatives to coring methods are explored in Berner et al. [7], which analysed drilling techniques for mining robots that could be adapted for sample collection. While mining often focuses on removing large amounts of material without preserving its structure, saw cutting could be employed for Mars sampling as a potential alternative to coring.

Zhang et al. [8] further analysed the potential of saw cutting for space rock sampling, proposing a robot designed for asteroid anchoring and sampling. This system employed diamond cutting discs mounted on legs and a sampling arm. Comparative results suggested that saw cutting could be more efficient than drilling, likely due to easier removal of rock fragments from the contact area. The proposed design allowed the robot to make four

cuts to obtain a square pyramid-shaped rock sample, which would then be grasped by a gripper. Its lightweight design makes it more feasible for UAV-based applications, though a caching system would be necessary to collect the samples after cutting. Figure 3 depicts this concept below.

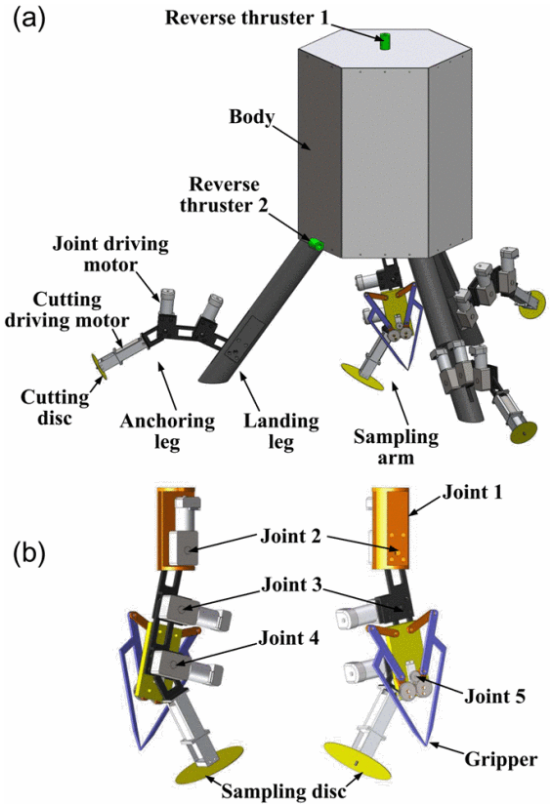

Figure 3 CAD model of the (a) robot with anchoring capabilities, and (b) the sampling arm [8].

2.3 Related Work on End Effector Designs

A variety of robotic gripping methods were explored by Hernández et al. in [9], focusing on different grasping modes such as parallel/flat, spherical, and cylindrical, which depend on the shape of the objects being grasped. The authors also distinguish between completely constrained and compliant gripper mechanisms. Constrained systems, which utilize rigid links, can precisely follow a planned path but struggle with complex objects, often requiring additional degrees of freedom (DOF). In contrast, compliant mechanisms rely on elastic deformation, making them lighter and simpler but potentially weaker. The paper also discusses underactuated mechanisms, which possess more DOF than actuators, facilitating adaptability to unfamiliar objects. These mechanisms often use passive actuation through springs or compliant materials, with notable designs such as origami grippers and fin-ray structured grippers presented in this paper.

A specific application of compliant materials and underactuation is seen in the fin-ray structured finger analysed by Pledger et al. in [10]. This design employs a wedge-shaped structure made of compliant materials like TPU. The researchers varied characteristics such as rib thickness, spacing, and angle to assess their impact on gripping ability. Results indicated that increased rib density enhanced object contact force while decreasing contact area. Conversely, reducing rib angle improved the enveloping grasp by allowing greater variation along the finger's length without significantly affecting contact force. Further optimisation of fin-ray structures was undertaken by Srinivas et al. in [11], where different

strut designs were tested for their wrapping capabilities. The study highlighted that straight slot struts performed well, especially at longer lengths, while thicker struts exhibited lower wrapping capabilities due to increased stiffness and resistance to deformation. Examples of these fin-ray structured fingers are shown below (Figure 4).

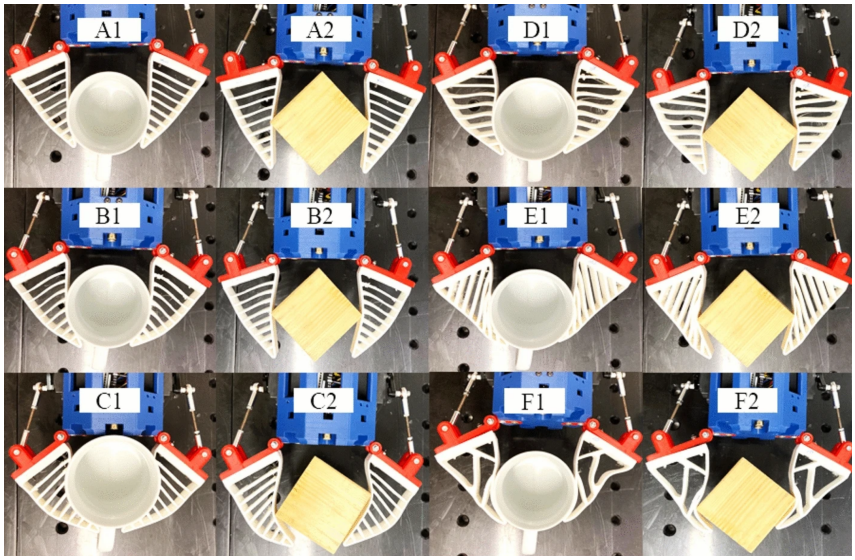

Figure 4 Demonstration of grasping capabilities of different fin-ray structured fingers [11].

Robotic mechanisms for grasping various materials in space were described by Spenko et al. in [12], identifying three main techniques: gecko-inspired adhesives, electrostatic adhesion, and microspines. Gecko-inspired adhesives enable easy release from surfaces by altering the loading direction, but manufacturing limitations restrict their complexity. Electrostatic adhesion utilizes electric fields created by electrodes embedded in a dielectric, offering dust-repelling capabilities but requiring high voltages, which pose safety concerns. Microspines function similarly to gecko adhesives, gripping objects under shear loads while allowing for release when the loading direction is reversed. However, their current applications have primarily focused on climbing rather than rock sampling.

Another innovative approach for rock sampling combines a rotary-percussive coring drill with a microspine gripper, as described by Parness et al. [13]. This gripper features 256 sharp steel hooks embedded in flexible frames (Figure 5), enabling it to support substantial weight while adapting to the irregularities of rock surfaces through passive degrees of freedom. Additionally, the development of a non-polymer-based prototype optimized for cold temperatures retained a high level of performance. One failure mode with the integrated drilling mechanism was wandering of the drill bit, which could cause the gripper to release unintentionally. This issue was similarly faced by the Perseverance Rover and solved with force exerted onto the surface by its robotic arm.

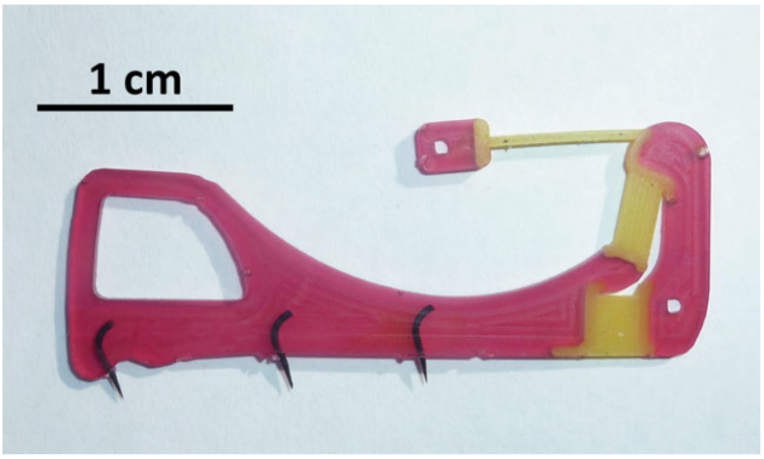

Figure 5 Microspine element with rigid frame, elastic flexures and embedded steel hooks [13].

A similar microspine gripper, inspired by the design described above, was developed for deep-ocean rock sampling [14]. The JPL-Nautilus Gripper was not only designed for anchoring and climbing on rock surfaces but was also designed and tested for object grasping. This design utilised linkages, each containing a sharp curved spine, arranged radially around a palm. Grasp testing involved the use of spherical objects that also included small and large rock samples (both exceeding 1kg in weight) and was largely successful even when tested with some lateral position error. However, smoother surfaces (such as a golf ball and baseball) were more difficult for the spines to grasp, and the larger rock's shape also prevented the gripper from scooping up the sample and ensuring a more secure hold. To improve this, the researchers suggest changing the spine contact angle as well as the linkage's finger tip geometry to better scoop under objects.

For collecting already cut or loose rock samples on Mars, an underactuated gripper designed for lunar rock was presented by Li et al. in [15]. This 3-fingered gripper can handle larger rocks, ranging from 100 to 200 mm in diameter, while reducing weight and complexity. Each finger's design includes barbs to increase frictional contact as seen in Figure 6, which could potentially be enhanced by incorporating compliant mechanisms such as microspines. This underactuated design, along with its kinematic analysis, offers promising capabilities for efficient rock caching.

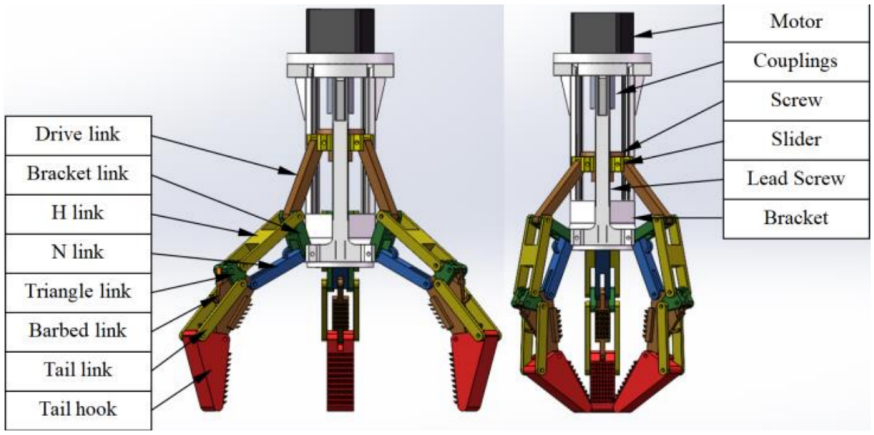

Figure 6 Structure of the underactuated gripper with barbed links [15].

2.4 Discussion of Related Work

The existing literature highlights various design concepts for sampling mechanisms, often dividing systems into two modules that each address a key aspect of the sampling process: 1. cutting and 2. handling or caching (carried out by a gripper or similar end effector). The designs for these two modules are discussed below with consideration given for the characteristics of the desired rock for sampling as summarised in Section 2.1:

Cutting Tool Design: Current methods such as coring are not well-suited for collecting features like digitate structures, as they risk damaging the internal structure of the target protrusions. Drilling presents a less invasive alternative but can still compromise the surface integrity, albeit over a smaller area. A more promising approach could involve saw cutting at an angle, which may facilitate the collection of samples while preserving the essential characteristics of the rock surface. This technique could be particularly beneficial in this case, where maintaining the integrity of the rock's surface features is critical for analysis.

End Effector Design: The literature indicates that underactuated systems are prevalent in current designs for sampling tools, allowing for reduced weight and complexity which is beneficial for both UAV integration and for payloads being sent to space. End effector concepts such as those utilising microspines are typically employed in larger rock sampling applications; however, their design presents challenges with handling smaller features such as the digitates of interest in this paper. Material compliance, as seen in the fin-ray structured fingers discussed in this report, is of interest as it could allow for adaptation to unique rock morphologies, accommodating the varying characteristics of the target rocks.

Overall, aspects of the sampling mechanism concepts previously discussed have advantages that could be adapted for use in sampling the rock of interest. However, given that none of these concepts provide solutions specifically targeted towards collecting the surface digitates, this gap in research necessitates the development of a novel system for rock sample collection of silica sinter deposits on Mars.

3. Design of End Effector for Rock Sample Collection

3.1 Design Considerations

3.1.1 Chosen Size and Shape of Rock Sample

Given that the surface digitates are the target of analysis, the tool will aim to sample a triangular pyramid by performing three cuts with a saw blade into the rock face, similar to the method outlined in [8]. This shape was chosen to minimise the number of cuts needed while also maximising the surface area of the rock collected. In order to be large enough to include multiple protrusions, a triangular pyramid with a side length of 69.3 mm (inscribed circle diameter of 40 mm) was chosen. The depth of the sample collected (thus the height of the pyramid) is less significant for collecting the digitates: the sample need only be deep enough by at least a centimetre to avoid fracturing the digitates. Thus, the depth was chosen to be 20 mm to allow for a cutting angle of 45 degrees.

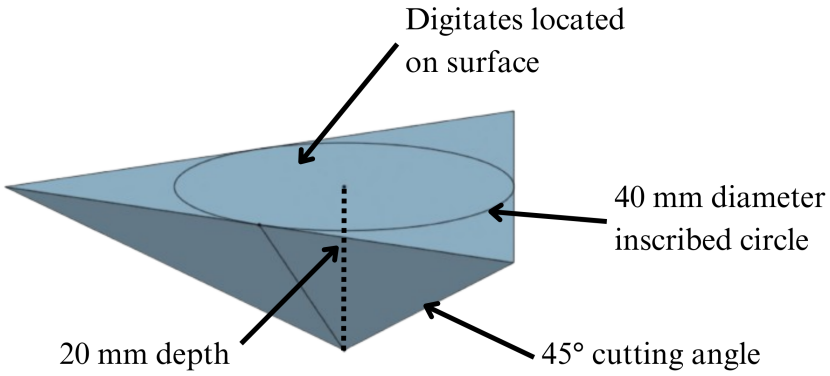

Figure 7 Chosen rock size and shape for sampling.

3.1.2 Design Considerations for Overall Sampling Mechanism

From analysis of related works and their conceptual designs, the sampling mechanism was divided into two main modules: a cutting tool and a grasping/collecting tool. This chosen modularity allowed for parallel development of the overall sampling mechanism as well as independent validation of the design concepts chosen for each system. Both modules were developed with the rock size and shape requirements, as well as each others' concepts, in mind and are described briefly below:

Cutting Tool Design: A circular cutting disc was chosen to perform the 3 cuts required to extract the sample. A swinging arm would drive the disc into the rock face at an angle of 45 degrees to horizontal. After this movement was complete and one cut formed, the entire system would rotate 120 degrees and perform two more cuts in this manner.

End Effector Design: The end effector would be located in the centre of the cutting tool in order to be centred above the sample being cut. This system would then perform the grasping procedure to scoop the sample out of the rock face. Thus, the end effector's diameter was required to be minimised to fit within the diameter of the cutting mechanism.

3.1.3 Design Considerations for End Effector

The end effector's specific design considerations were influenced by the chosen shape of the rock sample as well as its characteristics outlined in Section 2. These requirements are outlined below:

- The end effector must grasp and collect a triangular pyramid shaped rock sample out of the rock face which it is cut from,
- The end effector must be able to handle numerous broken pieces that may have been loosened or ejected during the cutting process,
- The end effector must not damage the sample's surface where the digitates are located,
- The end effector should be underactuated to minimise weight and complexity,
- The end effector must have added compliance to adapt to variability in the rock morphology.

3.1.4 Design Considerations for UAV Platform

A "black-box" approach was taken when considering the design of the system for a UAV platform. Essentially, given the modular design approach taken for the sampling mechanism, the system was designed to be mounted as a payload on most UAV platforms. This approach allows the system to be scaled depending on the platform and required configuration, or even if the planned sample size for analysis was changed.

The system is designed to be mounted underneath a typical UAV platform, such that sampling would take place on the ground directly below the UAV. This sampling method was chosen due to the rock deposits' location on the ground surface of Mars [6]. Thus, the UAV would land on the ground surface to ensure stability of the sampling mechanism before cutting, and would thus need to orient the system perpendicular to the rock face.

3.2 Mechanical Design of End Effector

The mechanical design of the end effector is outlined in this section and depicted in Figure 8 below. The design is split into three main parts: the spiral-driven arm mechanism, the linear motion mechanism and the shovel-inspired fingers. These parts are discussed in more detail in their respective sections. The overall concept of the end effector design is described below.

To grasp the triangular pyramid sample from the rock face, the end effector was designed to utilize the cut lines made by the cutting tool. The fingers were angled at 45 degrees to horizontal (i.e. the rock face) and made thin at the tips to follow the cut lines precisely. Actuation was thus required to move the fingers linearly downward and radially inward at a constant rate, achieved by the spiral-driven arm and linear motion mechanisms. Three fingers were used, each shaped like the sides of the sample and made larger than the sample size to enclose any broken pieces displaced during cutting. This side-grasping approach prevents damage to the sample's surface and allows it to be lifted out once fully encased.

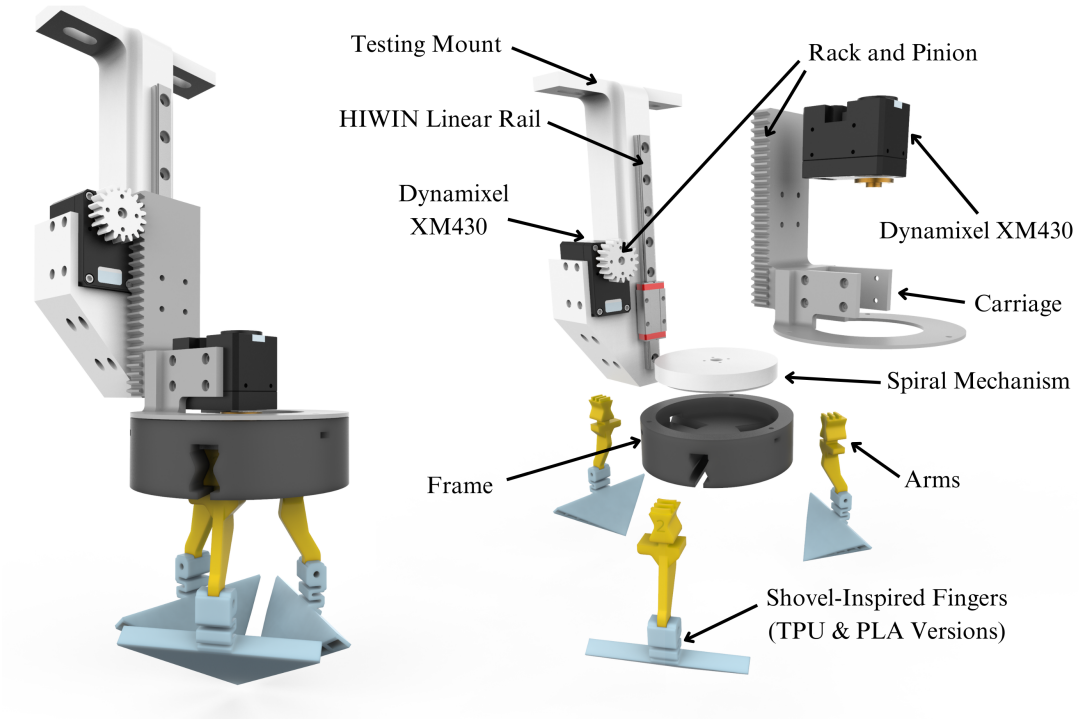

Figure 8 Exploded view of end effector design.

The overall weight of the end effector is very light at 0.47 kg (excluding small hardware such as screws and nuts). A table of parts is included below (Table 1).

Part Name	Weight (g)	Quantity
Spiral-grooved disc	24.68	1
Arm	3.75	3
PLA or TPU finger	10.73 or 11.39	3
Disc frame	61.12	1
Carriage/plate/motor mount	38.24	1
HIWIN 150 mm linear rail	60	1
24.75 mm pinion gear	2.99	1
Linear slider/motor mount	79.13	1
Dynamixel XM430-W350	82	2

Table 1 Mechanical parts list for end effector prototype.

Based on this chosen concept, the list of operations of the end effector integrated with the cutting mechanism and UAV platform are as follows:

1. The UAV platform lands on the desired sample for collection, aligning the system perpendicular to the ground,
2. The cutting tool moves the swinging arm with the spinning saw blade into and out of the rock face to perform one cut,
3. The cutting tool rotates the entire swinging arm with the attached saw disc 120 degrees into its new position,
4. Steps 2-3 are repeated twice more to fully cut a triangular pyramid shaped sample from the rock face,
5. The end effector moves linearly downwards until just above the rock face, with all three fingers extended to align with the cut lines,
6. The end effector moves linearly downwards, and the arms radially inwards, at a constant pre-defined rate to move the fingers along the cut lines,
7. Once the fingers complete their full range of motion and the sample is fully encased, the end effector moves linearly upwards to lift the sample out of the rock face, thereby completing the sampling procedure.

3.2.1 Spiral-Driven Arm Mechanism

To enclose three sides of the triangular pyramid shaped sample simultaneously, the three fingers of the end effector must move radially inwards together. An Archimedean spiral-driven mechanism, inspired by a 3-fingered rotary module developed for a gripper in [16], was chosen to accomplish this due to its underactuated nature and simple kinematics.

The mechanism consists of:

- a disc with a spiral groove on its underside,

- three arms attached to the end effector fingers, each with three curved teeth to mesh with the spiral groove on the disc,
- a frame to encase the disc and provide radial constraints for the three arms,
- a plate (attached to the carriage for the linear rail, discussed later in this report) to keep the disc contained in the frame,
- a Dynamixel XM430-W350 [17], mounted to the linear rail carriage, attached to and driving the rotation of the disc.

All parts excluding the motor were 3D-printed in PLA to rapidly prototype and iterate the design as well as reduce weight. Hardware such as screws were used to attach parts together and provide physical stops for the arms, while washers were used to provide enough clearance for the disc to spin freely within the frame. The Dynamixel motors were chosen for their high torque capabilities, lower weight and their availability in the lab.

The spiral grooved disc's diameter, chosen to be 80 mm, was required to be as small as possible for the end effector to fit within the cutting tool design. However, the travel distance of each arm on the disc was required to be at least 20 mm to achieve enough range of motion for fully encasing the sample. The middle of the disc contained screw holes instead of spiral grooves so that it could be mounted onto the Dynamixel motor. These attributes led to the specific dimensions chosen for the spiral and are described in Section 3.3 alongside the end effector kinematics.

This spiral mechanism was chosen to actuate the end effector's fingers over other techniques, such as a four bar linkage mechanism, due to its simplicity and fewer moving parts. Screwing or drilling into the rock sample to grip it internally was also considered, but this could damage the digitates on the surface and may result in the sample breaking apart. Furthermore, the spiral mechanism works well for radially expanding and retracting three or more arms without the need for additional actuators as proven through validation of the concept in [16].

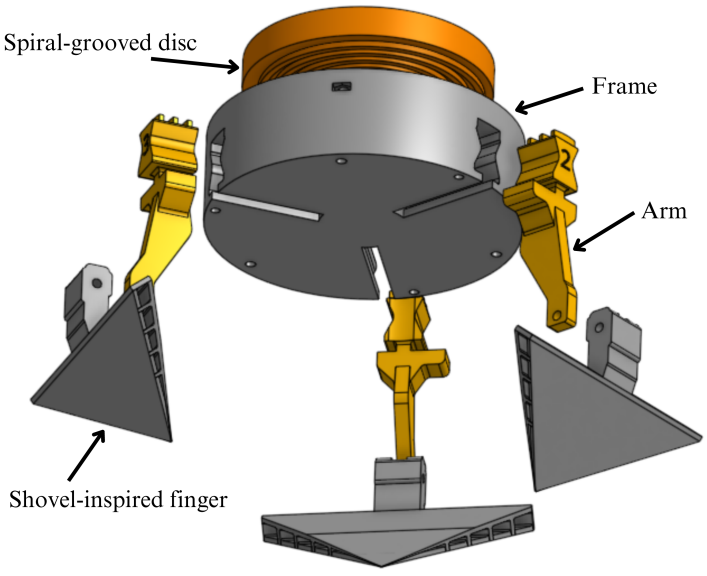

Figure 9 CAD design (exploded view) of spiral-driven mechanism for radial movement of fingers.

3.2.2 Linear Motion Mechanism

To actuate the linear portion of the gripping motion, as well as the motion required to lift the rock out of the rock face, a rack and pinion was used with a carriage mounted to a linear rail. The parts involved include:

- a pinion gear with pitch diameter of 24.75 mm,
- a Dynamixel XM430-W340 to actuate the pinion gear,
- a HIWIN linear rail,
- a 3D-printed mount to hold the pinion gear Dynamixel motor and the linear slider, and to attach to aluminium extrusion for validation,
- a 3D-printed carriage to mount onto the rail, which includes the rack, a mount for the Dynamixel motor actuating the spiral disc, and the plate mounted onto the frame of the spiral mechanism.

To develop a prototype for testing, the spiral-driving motor was offset from the carriage to reduce the height of the aluminium extrusion needed for the testing rig discussed later in this report. The rack and pinion gear drive was chosen for its simplicity due to the nature of the kinematics needed for driving the fingers into the rock face (described further in a later section).

3.2.3 Shovel-Inspired Fingers

The three fingers of the end effector must be shaped appropriately to envelop and lift the rock from its three sides. The shape and motion of the fingers is thus inspired by a shovel, but shaped as a triangular wedge to match the side of the sample. These fingers are also sized larger than the sample in order to better encase rock pieces dislodged during cutting, and are oriented 45 degrees to horizontal to align with the cut lines. The wedge design, where the fingers start thin at the bottom and gradually increase in thickness up to the arm, allows the rock to become dislodged from the ground as the fingers push between the sample and the rest of the rock.

Multiple different 3D-printed iterations of the fingers were created, resulting in two main designs (shown in Figure 10 below):

- a PLA-based design with a compliant hinge,
- a TPU-based design inspired by fin-ray structured grippers.

These two designs were chosen for validation due to differences in their material properties, with PLA being a more rigid, smooth material and TPU a more compliant material. Material considerations are discussed further in the next section of this report.

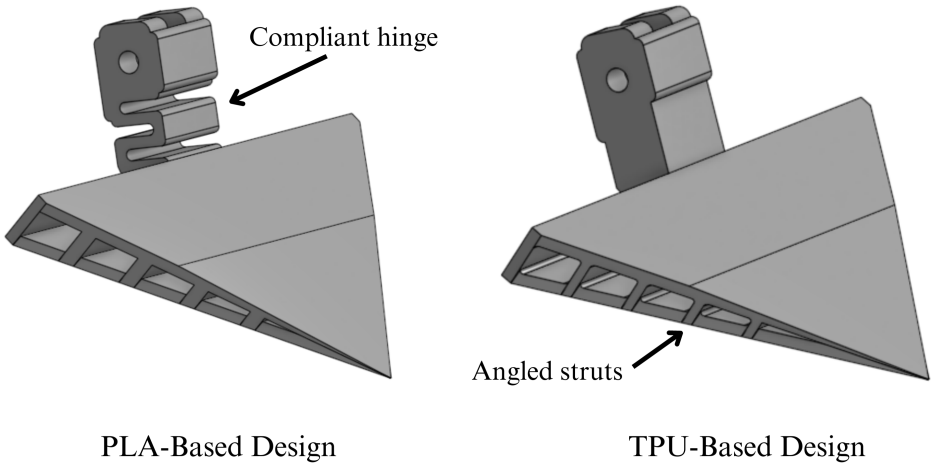

Figure 10 PLA-based and TPU-based shovel-inspired finger designs.

Compliance, either through the hinge design or material choice, was necessary due to the underactuated nature of the end effector mechanism and unpredictable nature of the rock morphology. If one finger encounters the side of the rock sample before the other two, this finger must have some natural "give" while the other fingers are actuated until they reach the sample as well.

The design of the TPU fingers specifically was based on fin-ray structures discussed in Section 2 [10] [11]. This particular structure was chosen for its passive actuation through material flexibility, allowing the finger to mold to variable surfaces such as a rock face while still maintaining stiffness and strength. TPU is a naturally compliant material, so in order to achieve the necessary stiffness for the material to lift the rock sample, 1.0 mm-thick angled struts were placed within the structure of the finger. These struts were oriented perpendicular to the surface of the finger (and thus the rock side being grasped) to maximise stiffness while lifting the rock.

3.2.4 Material Consideration for Finger Design

In considering the Mars application of this design, material choice is especially notable given the differing conditions on Mars compared to Earth. The glass transition temperature of TPU is typically between -20 and -50 degrees Celsius [18], allowing the material to be flexible at room temperature on Earth. However, with a surface temperature that can vary between 20 and -153 degrees Celsius on Mars [19], TPU would likely become brittle as temperatures are likely to dip lower than its glass transition temperature. Although the lack of atmosphere on Mars would decrease the glass transition temperature slightly [20], such an effect would likely be minimal compared to the influence of the extreme cold temperature. Thus, on Mars, TPU would likely behave similarly to PLA on Earth, lose its compliance, and possibly become brittle enough to fracture. However, other compliant materials could be used in replacement of TPU that may maintain their flexibility at extremely cold temperatures.

PLA, unlike TPU, has a high glass transition temperature of around 55-60 degrees Celsius [21]. Given that PLA already operates in a brittle state at room temperature, its performance would significantly degrade at cold temperatures, thereby losing all strength and likely shattering under load. A material with a lower glass transition temperature such as TPU could therefore perform more effectively with the PLA design on Mars. However, to fully

maximise strength and potential compliance, a metallic material would likely perform best. Despite the inherent flaws of using TPU and PLA filament, their finger designs are still worth investigating and validating and can be replaced with more suitable materials in future development.

3.3 End Effector Kinematics

The spiral used to control the radial position of the shovel arms can be approximated as an Archimedean spiral. In polar coordinates, the radial position of a point on one of these arms can be described by the following equation [22]:

$$r = a\theta_1 \tag{1}$$

where r is the radial position (mm) of the point along the disc from its centre point, θ_1 is the angular position (rad) of the point along the spiral, and a (mm/rad) is a constant denoting how tightly wound the spiral is. Given the spiral dimensions used for the current end effector design, a was found to be approximately equal to 0.75 mm/rad by graphing the spiral in Desmos and aligning it with key points from the CAD model (Figure 11). The Desmos tool made for this analysis can be found here: https://www.desmos.com/calculator/jlgnzibdfq.

From here, the radial velocity $\dot{r}$ (in mm/s), and hence the velocity of each arm due to their radial constraint, is given by differentiating the above equation to give:

$$\dot{r} = 0.75\dot{\theta_1} \tag{2}$$

where $\dot{\theta_1}$ is the rotational velocity of the motor driving the spiral.

In order for the shovels to extend into the rock face along the cut lines, which are at a 45° angle from the rock face, the vertical velocity $\dot{y}$ (in mm/s) of the end effector system as provided by the linear rail must equal:

$$\dot{y} = \frac{\dot{r}}{\tan(45°)} = 0.75\dot{\theta_1} \tag{3}$$

Thus, using a pinion gear pitch circle diameter of 24.75 mm, the relationship between the pinion gear motor rotational velocity ($\dot{\theta_2}$) and ($\dot{\theta_1}$) is:

$$\dot{\theta_2} = \frac{2}{24.75}\dot{y} = \frac{2 * 0.75\dot{\theta_1}}{24.75} = 0.06\dot{\theta_1} \tag{4}$$

Velocities for both motors were chosen with these kinematics in mind and are discussed further in Section 4 below.

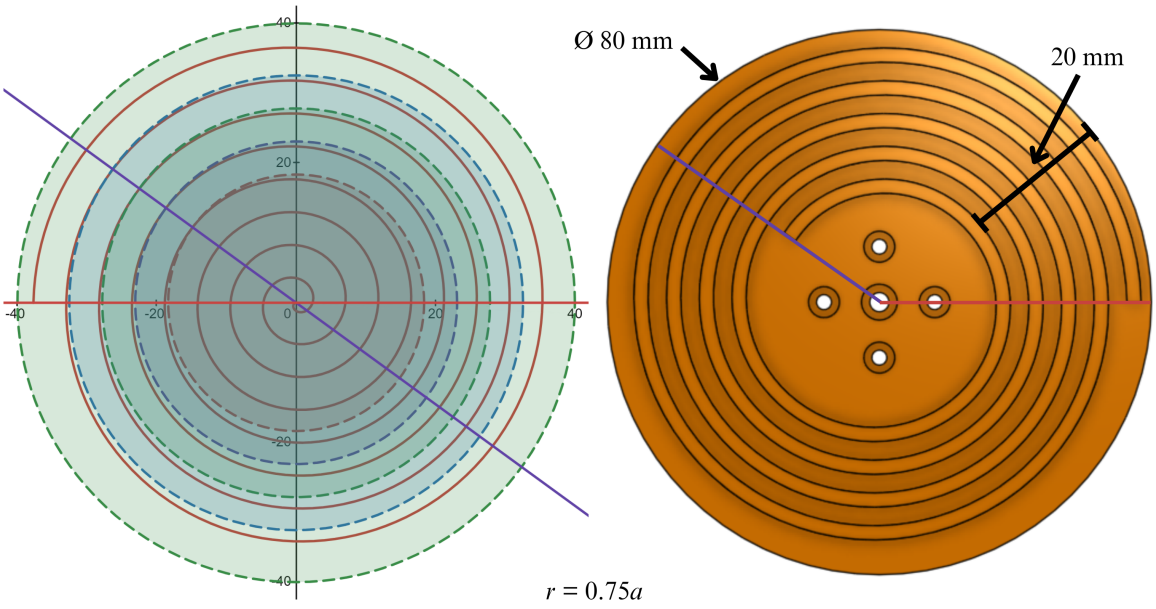

Figure 11 Graphical representation of Archimedean spiral design.

4. Methodology and Experimental Validation

4.1 Validation Methods

To select experimental methods for validating the rock sampling end effector, related works and their validation methods were analysed and discussed. One such work is a three finger variable stiffness gripper [23], whose performance was validated using five experimental benchmark tests adapted from the National Institute of Standards and Technology's Finger Strength Test [24]. These tests were developed exclusively for variable stiffness grippers, but still have relevance for other gripper types. The tests were as follows: 1. object grasping test, 2. finger force test, 3. grasp strength test, 4. gripper payload test, and 5. gripper slip resistance. Of particular note are the object grasping test, which determines the variation in object shapes and sizes that the gripper can grasp, and the grasp strength test, which analyses the strength that grasped objects experience. Tests such as the gripper slip resistance test are out of scope for the proposed design as the goal is to scoop underneath the sample rather than to hold it on all three sides.

Another relevant example is a soft enveloping gripper from [25], which underwent static grasping and dynamic stability tests to validate the design. Static grasping involved a permissible position error test, where an object was placed in 31 different locations and 50 grasping attempts made at each position. This method of testing allowed the gripper to be analysed for its robustness against positional errors (the error in placement of the object with respect to the gripper), and would be of use validating the proposed end effector design in this report due to the possibility of gripper or sample displacement during the cutting process. Dynamic stability involved picking up an object and moving it at different speeds, then suddenly stopping. the resulting vibration of the object is then recorded by a high-speed camera and its displacement recorded. Given the nature of the proposed end effector's collection mechanism (designed to move at slow speeds), and for ease of setup, this method was also determined to be out of scope.

Finally, validation of fin-ray structured end effectors was carried out in [11] and [10], where variables such as stiffness, deflection, distribution of contact pressure, and contact area with

the grasped object were analysed. The latter work also analysed the effect of varying aspects of the fin-ray structure such as rib thickness, rib spacing and rib angle, thereby affecting the stiffness of the design. Contact area in particular was significant for analysing the grasp effectiveness of these designs and is also relevant to the proposed design in this report.

Based on the above related works for validation methods of end effectors, the following validation methods were chosen for the end effector proposed in this report:

1. Grasping ability of PLA and TPU fingers on a variety of rock samples of differing weights, morphologies and degrees of brokenness,
2. Grasping ability of either the PLA or TPU fingers (whichever one is better performing in the previous tests) with different positional errors of the sample with respect to the end effector.

These tests were chosen to verify the end effector's ability to enclose and collect rock samples that could vary in their morphology from the cutting process. The exact sample shapes and sizes that were prepared for testing are discussed later in this report. The PLA and TPU designs were chosen to be compared given their respective advantages and disadvantages, as well as their differing material properties and their implications for use on Mars. Given the chance of misalignment of the end effector due to vibrations and other forces from the cutting tool, testing with different sample positional errors will also evaluate the end effector's robustness in its projected application.

4.2 Experimental Procedures

The sampling procedure is divided into two segments: scooping and lifting. Scooping is the portion of sampling where the fingers move radially inwards while the end effector moves downwards to encase the sample. Lifting immediately follows scooping and lifts the encased sample out of the sample bed. The end effector does not need to have completed a successful scooping segment to achieve a successs in lifting for the same trial.

Six different rock samples, described in the Rock Samples section below, will be tested with both the PLA and TPU fingers to compare their performance with grasping rocks of different morphologies. 10 trials will be conducted per sample and the overall success rate for that sample recorded as a percentage of successful grasps out of total trials conducted. In the case of broken samples, the success rate will be captured as a percentage for each trial based on the percentage of the original sample's weight that was successfully collected. For example, if the amount successfully collected in a trial is 50% of the original weight of the sample, the success rate recorded for that trial will be 50%.

For the positional error tests, one rock sample will be tested with the best performing finger from the previous tests. The sample bed will be moved with respect to the end effector to create the positional error (previous tests will have otherwise been conducted with the sample bed centred underneath the end effector). Three different were chosen for testing: a lateral offset of 3 mm in the x axis, a lateral offset of 3 mm in the y axis, and a rotational offset of 3 degrees clockwise (CW) in the z axis. 3 mm was chosen because, during tests of the cutting tool, the thickness of the cuts made was approximately 3 mm. Thus, an offset of 3 mm would be necessary for the end effector to handle in its proposed application as the sample could be displaced by this amount during cutting.

The experimental procedure is as follows:

1. Measure weight of rock sample before placing in testing bed.
2. Perform scooping motion (encasing sample with fingers).
    - If spiral motor speed falls below 0.5 rpm for at least 5 seconds before completing the fingers' full range of radial motion, stop scooping and record result as a fail, but do not remove the rock from the sample bed.
    - If spiral motor doesn't stall until fingers successfully complete the full range of radial motion, stop scooping and record result as a pass, but do not remove the rock from the sample bed.
3. Perform lifting motion and hold rock for 10s in a position above and clear of the sample bed.
    - If rock falls out of gripper during motion or after 10s of holding, record result as a fail (0% collected).
    - If rock successfully stays entrapped, record weight of rock collected as a percentage of the starting weight of the sample.
4. Repeat steps 1-3 for a total of 10 trials per sample.

4.3 Test Setup

4.3.1 Mechanical Design of Testing Rig

To perform the above validation tests on the sampling tool, a testing rig was created to keep both the sample and end effector secured. Slots for M8 screws were added to the frame holding the linear slider and the pinion gear motor such that the end effector could be mounted in a vertical position, similar to its goal of being mounted underneath a UAV.

The testing rig was constructed with aluminium extrusion and 3D-printed brackets, with a wide base to minimise movement and vibrations during testing. A triangular cup, the size of the target sample being cut, was 3D-printed and screwed into an acrylic base and placed at the bottom of the testing rig. 5mm offset slots were also included in the cup, allowing the sample to be both centred underneath the end effector or offset by a small amount along the x or y axes for positional error tests. These slots also allow for a small rotation of the sample bed so that rotational error about the z axis can be tested.

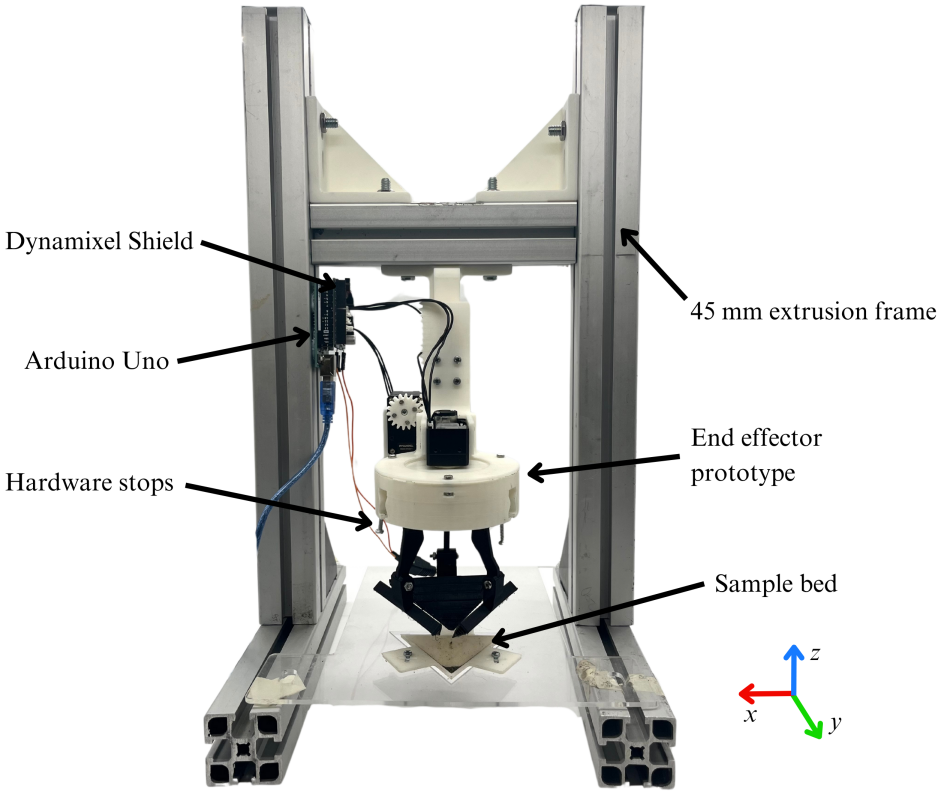

Figure 12 Testing rig for experimental validation.

4.3.2 Electronics and Software Design

To power and control the two Dynamixel XM430 motors used for the prototype, an Arduino Uno and Dynamixel Shield was used and powered by a 12V, 1.5A power source.

The software to run the testing program was based on a Dynamixel-developed script for velocity control of the motors [26]. This program was developed with a finite state machine structure to carry out the scooping and lifting motions:

- The first state, SCOOP, starts upon reset of the Arduino Uno and carries out the scooping motion. The spiral motor is set to -30.0 rpm and the pinion gear motor is set to 1.8 rpm, causing , causing the arms to move radially inwards and the end effector to move downards at equal speeds of 2.36 mm/s. Together, this causes the fingers to close at a constant rate such that they follow the 45 degree cut lines to enclose the sample.
- The second state, LIFT, is entered if the spiral motor speed falls below 1.0 rpm for more than 5 seconds. In this state, the spiral motor speed is set to 0.0 rpm and the pinion gear motor is set to -1.8 rpm to lift the end effector with the fingers enclosed around the sample.
- The third state, STOP, is entered after the program has been in the LIFT state for more than 12 seconds. All motors are set to 0.0 rpm in this state.

The above motor speeds were chosen to ensure the system would move slow enough so as to avoid damaging mechanical components or the rock samples themselves. The code developed for this test can be found in Appendix A.

4.4 Rock Samples for Experimental Validation

Five rock samples were initially prepared to test various morphologies and levels of brokenness. Sandstone from a local Auckland beach was used due to its friability and dust production. These characteristics thus simulate one of the worst case scenarios for the rocks on Mars: rocks that might easily break apart during cutting or release large amounts of dust that could be hard to clean off components.

The triangular cup, which formed the sample bed, served as a reference for shaping the rocks to roughly match the target sample. This was done using a hammer and chisel, but exact shapes weren't achieved, leaving many faces rough and with sharp edges. These irregular morphologies simulate challenges the end effector might face if the cutting tool can't produce a smooth cut or pieces break prematurely. Three unbroken samples were prepared with different weights, and two others were intentionally broken into 3 and 6 pieces to simulate samples potentially fractured during cutting. A maximum of six pieces were chosen as more fragmented samples would likely lack unbroken digitates for analysis.

A sixth sample was cut using the cutting tool developed as part of the overall sampling mechanism. The sample was cut in one whole piece and with generally smooth side faces, unlike the other five samples prepared for testing. This sample was not cut at full depth due to the design of the prototype for testing, so its dimensions are smaller than the planned sample size. However, the shape of the sample closely resembles the planned shape for cutting and is thus ideal for testing with the end effector. For this reason, the sample was also used for the positional error tests. The top triangular face has dimensions of 45 x 40 x 40 mm, and the sample has a depth from base to tip of 15 mm.

An image of the prepared samples is shown below (Figure 13). The characteristics of these samples are detailed in Table 2 excluding the size of sample six (described above).

Figure 13 Image of rock samples prepared for experimental validation.

Sample No.	Weight (g)	Amount of Brokenness	Size (w x l x d, mm)
1	31	Whole piece	35 x 46 x 25
2	42	Whole piece	37 x 38 x 26
3	55	Whole piece	48 x 43 x 25
4	33	3 pieces	43 x 47 x 20
5	41	6 pieces	55 x 49 x 22
6	16	Whole piece	See above description

Table 2 Characteristics of rock samples prepared for experimental validation.

5. Results

5.1 PLA vs. TPU Fingers

Results from the grasping tests, averaged across all 10 trials, with the six different sample types and both PLA and TPU fingers are shown in Table 3 below. Generally, scooping success rate was very poor for both finger types, with the end effector unable to complete the full range of motion in most trials. Reasons for this are discussed in the Discussion section below. However, the PLA fingers were slightly more successful with completing the full range of motion when scooping sample 6.

Despite poor scooping success, the lifting segment saw a higher success rate for both finger types, especially for unbroken samples which had a 100% success rate when sampled by the PLA fingers. Samples that were not fully scooped and enclosed were still able to be lifted out of the testing bed, such as with sample 1 which had a 100% lifting success rate despite a 10% scooping success rate for both finger types.

The PLA fingers had a higher success rate with collecting whole samples, including sample 6 which most closely resembles the target shape. In contrast, the TPU fingers had a lower success rate with whole samples, more significantly so with sample 6. With the broken samples, however, the TPU fingers had a slightly higher success rate compared to the PLA fingers, corresponding to a greater percentage of rock sample collected per trial.

Sample No.	PLA Fingers Scooping Success Rate	PLA Fingers Lifting Success Rate	TPU Fingers Scooping Success Rate	TPU Fingers Lifting Success Rate
1	10%	100%	10%	100%
2	30%	100%	30%	80%
3	10%	100%	10%	80%
4	0%	52.42%	10%	68%
5	0%	61.95%	0%	63%
6	40%	100%	10%	60%

Table 3 Grasping test results for different samples and finger designs.

5.2 Positional Error Results

Due to the PLA fingers' higher performance in the first set of tests described in the previous section, these fingers were chosen for the positional error tests with sample 6. The results of these tests are shown in Table 4 below. Similar scooping success rates were seen in all three positional errors, while lifting success rate was higher for the linear offsets compared to the rotational offset. The lateral error in the x axis also had the highest success rates in both the lifting and scooping segments compared to the other two offsets tested.

Axis of Offset	Amount of Offset	PLA Fingers Scooping Success Rate	PLA Fingers Lifting Success Rate
x axis	+3 mm	30%	60%
y axis	+3 mm	50%	80%
z axis	3 degrees CW	30%	40%

Table 4 Sample 6 grasping test results with positional error.

6. Discussion and Limitations

6.1 Causes of Grasp Success and Failure

A summary of the main causes for the success or failure of a grasp is shown below:

- If the rock was fully encased (i.e. full range of scooping motion achieved), the rock would be successfully lifted in all cases,
- If the rock was partially encased (i.e. all three fingers touched the rock on each side, but the spiral motor stalled prematurely), the rock would either fall during the lifting process if not encased enough, or would be successfully grasped,
- If a finger failed to wedge itself between the sample and the testing bed, the rock wouldn't be lifted at all due to a missing point of contact.

A key result from experimental validation is that, if the end effector was able to achieve full range of motion in the scooping segment, the lifting segment was guaranteed to be successful as well. However, if the fingers had only partially completed the scooping motion and maintained contact on all three sides of the rock sample, the sample could still be picked up and held in this position. Figure 14 demonstrates an example of this occurring and resulting in a successful grasp. Generally, a point of contact from each finger on the rock sample is needed for a successful grasp, but the sample need not be fully encased. Overall, a higher range of motion achieved during scooping directly corresponds to a more secure grasp of the rock and therefore a higher chance of successfully sampling it.

Main causes of failure during validation tests were due to the surface of the fingers catching on the sides of the rock, or otherwise failing to wedge itself in the space between the sample and the testing bed. Such failures resulted in the spiral motor stalling while the pinion gear motor still moved the end effector downwards. The fingers were occasionally able to free themselves in this scenario, allowing the spiral motor to continue turning and the fingers to continue encasing the sample. However, if the fingers were unable to free themselves after 5 seconds, the lifting motion would begin at whatever position the fingers were stuck in. From there, the rock would either be successfully grasped if encased enough, or it would fall/fail to be lifted.

An observation also worth noting is that dust and small particles from the rocks collected in the bottom of the sampling bed during testing. These particles were unable to be grasped by the end effector, but are not the subject of analysis for the rocks, so a failure to collect them is inconsequential for this application.

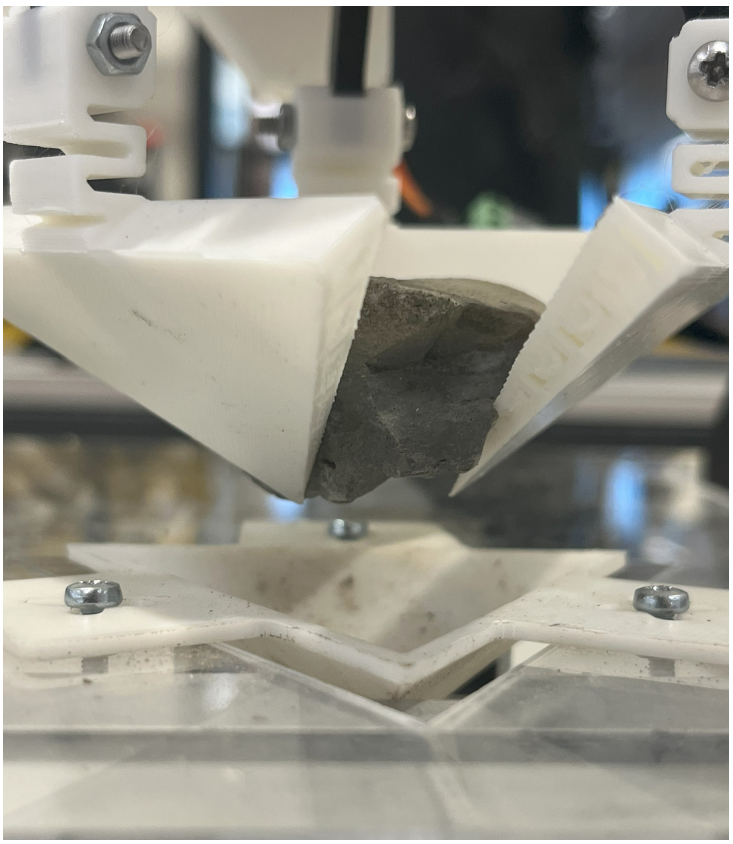

Figure 14 Image of partially encased sample that was successfully lifted during validation tests.

6.2 Impact of Finger Design on End Effector Performance

From the experimental tests comparing the PLA and TPU fingers, the PLA fingers were found to perform better when carrying out the scooping segment of the sampling procedure on unbroken samples. Although the full range of motion was rarely achieved with all samples, the PLA fingers were able to complete slightly more range of motion through sliding the fingers further along the space between the sample and testing bed. This success was especially seen with the rock acquired using the cutting tool, showing that the PLA fingers are more effective at picking up the target rock. Reasons for this better performance are likely due to the PLA fingers' lower friction on the surface contacting the rock face, allowing the fingers to move further along before catching on any sharp edges.

The TPU material, on the other hand, would catch more often on sharp edges due to its higher friction. This characteristic was desirable for the lifting segment, especially for broken pieces by preventing them from slipping (discussed further below), but prevented a more secure grasp from being achieved in the scooping portion. Additionally, the flexible and thicker nature of the TPU fingers' tips occasionally prevented a finger from wedging between the sample and sample bed (Figure 15), eliminating a contact point on one side of the sample and resulting in a failed grasp.

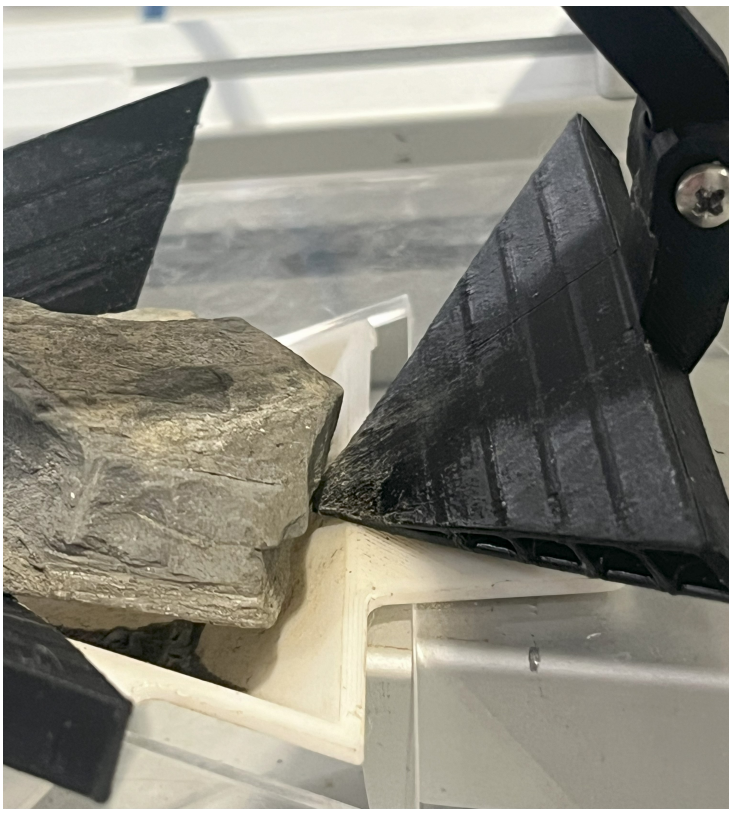

Figure 15 Edge of TPU finger bending instead of wedging between rock sample and testing bed, resulting in a failed grasp as no point of contact could be established on this side.

The TPU fingers, however, had a slightly higher success rate when sampling the broken rocks compared to the PLA fingers. This result is likely due to TPU's flexible material which allowed the fingers to better mold to the shifting pieces, preventing them from slipping and ensuring a stronger grasp.

Lastly, both fingers' inherent compliance (PLA through the hinge design and TPU through its material properties) were effective in scooping up the irregularly shaped rocks. The fingers were able to perform all trials without experiencing material failure, although one 3D-printed arm did experience shear failure in two places during testing and required replacement. This failure could be addressed with a different printing orientation and higher infill.

6.3 Impact of Rock Sample Characteristics on Performance

Overall, the end effector was able to successfully grasp rocks of varying morphologies and degrees of brokenness. However, with broken samples, it often failed to grasp all the pieces in a given trial, especially smaller ones at the bottom of the sample bed. This was usually due to the fingers getting stuck before completing their full range of motion, causing the motor to stall and the lifting segment to start prematurely. As a result, the ends of the fingers were never able to reach these pieces at the bottom of the testing bed (as seen in Figure 16). However, these smaller fragments would likely be undesirable for analysis as they wouldn't contain the digitates on the rock's surface, so this limitation may be acceptable for this application. Additionally, the sample cut using the cutting tool developed for this project did not fracture the rock, despite its friability, so it is reasonable to assume that there would be minimal to no breakage of the sample being collected.

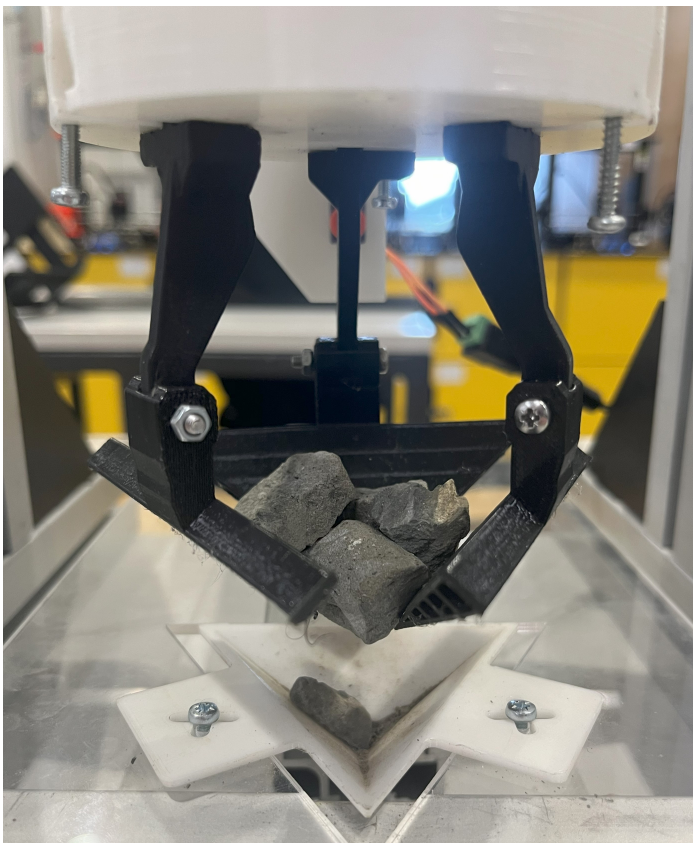

Figure 16 Broken piece at the bottom of the testing bed that failed to be grasped.

Similar failure rates were observed for both the PLA and TPU fingers, although the TPU fingers had a slightly greater success rate when lifting up the broken samples. This is likely due to the material's higher friction and the design's compliance, allowing a slightly better grip onto smaller pieces that often shift when being scooped or lifted.

6.4 Impact of Positional Error on Performance

Tests with positional error of the sample relative to the end effector had poorer results compared to the sample being centred. In most cases, this lower success rate was due to one or more fingers failing to wedge themselves between the side of the rock and the testing bed, preventing the end effector from proceeding further. If all three fingers were able to wedge into the cut, then the sample could often be re-oriented within the grasp of the fingers while being scooped. Another observation from the test results is that the offset in the y axis saw a higher success rate compared to the other offsets. This is likely due to the orientation of the sample with respect to the end effector: with a y axis offset, only one of the shovels was severely displaced from the rock side, whereas two were displaced with the x axis offset and all three displaced with the rotational offset about the z axis.

7. Conclusion and Suggestions for Future Work

The development of an autonomous sampling mechanism for collecting silica sinter geological samples is a crucial step toward the search for life on Mars. This project aimed to create a novel system capable of extracting and grasping rocks with varying morphologies, and the successful validation of the end effector's performance confirms its effectiveness in achieving this goal.

The end effector demonstrated the ability to grasp rocks with diverse shapes and sizes, as well as differing amounts of brokenness, with a relatively high success rate especially for larger pieces. Through doing so, the end effector has proven feasibility for grasping more porous or friable rocks such as the silica sinter deposits without damaging crucial surface features. A comparative analysis of the two finger materials and designs, PLA and TPU, showed the advantages of PLA fingers during the scooping phase of the grasping procedure. However, TPU fingers performed better with broken samples, showing that a hybrid design combining the strengths of both materials may further enhance overall performance. The feasibility of integrating the sampling mechanism with the cutting tool was also validated through successful grasping of the rock sample that was extracted by the cutting mechanism developed for this project.

Potential improvements to address the failures observed previously, as well as improve the performance of the end effector, are listed below:

- A combination of the two finger designs, with a compliant structure that can better mold to unique rock morphologies but with a more rigid, low friction tip to better enter the rock face and slide under sharp edges,
- A method of "propping up" the rock sample to expose all three cut lines, or otherwise ensuring space between the sample and rock face on all three sides,
- An improved scooping motion, where the spiral motor continues to move the fingers closed during the initial phase of the lifting segment, and/or moves the fingers closed for a tighter grasp before beginning the lifting segment,
- Strategically cutting the sample such that, after the cutting process displaces it to one side (as observed in tests of the cutting tool), it is displaced in a more favourable position for grasping (eg. with only one finger displaced).

Additional future work will focus on refining the end effector design for seamless integration with the cutting tool, addressing the above improvements, investigating methods for stabilising rocks during sampling, and integrating the overall system with a UAV platform. Overall, this project lays a solid foundation for future robotic missions on Mars, enhancing our understanding of the planet's geology and contributing to the search for signs of extraterrestrial life.

References

[1] Y. Gao and S. Chien, "Review on space robotics: Toward top-level science through space exploration," *Science Robotics*, vol. 2, no. 7, p. eaan5074, 2017.

[2] R. Anderson, L. Beegle, J. Hurowitz, C. Hanson, W. Abbey, C. Seybold, D. Liminodi, S. Kuhn, L. Jandura, K. Brown *et al.*, "The mars science laboratory scooping campaign at rocknest," *Icarus*, vol. 256, pp. 66–77, 2015.

[3] R. C. Moeller, L. Jandura, K. Rosette, M. Robinson, J. Samuels, M. Silverman, K. Brown, E. Duffy, A. Yazzie, E. Jens *et al.*, "The sampling and caching subsystem (scs) for the scientific exploration of jezero crater by the mars 2020 perseverance rover," *Space Science Reviews*, vol. 217, pp. 1–43, 2021.

[4] S. Withrow, W. Johnson, L. A. Young, H. Cummings, J. Balaram, and T. Tzanetos, "An advanced mars helicopter design," in *ASCEND 2020*, 2020, p. 4028.

[5] E. E. Nersezova, M. C. Rowe, K. A. Campbell, A. Ang, S. Matthews, S. W. Ruff, A. Meghwal, L. Adam, N. Galligan, and T. Loho, "Exploring the internal textures and physical properties of digitate sinter in hot springs: Implications for remote sampling on mars," *Planetary and Space Science*, vol. 238, p. 105786, 2023. [Online]. Available: https://www.sciencedirect.com/science/article/pii/S0032063323001551

[6] S. W. Ruff and J. D. Farmer, "Silica deposits on mars with features resembling hot spring biosignatures at el tatio in chile," *Nature communications*, vol. 7, no. 1, p. 13554, 2016.

[7] M. Berner and N. A. Sifferlinger, "Analysis of excavation methods for a small-scale mining robot," in *ISARC. Proceedings of the international symposium on automation and robotics in construction*, vol. 37. IAARC Publications, 2020, pp. 481–490.

[8] J. Zhang, A. Song, and W. Lu, "Anchoring and sampling processes analysis of a landing robot in asteroid exploration," in *2016 IEEE International Conference on Robotics and Biomimetics (ROBIO)*. IEEE, 2016, pp. 185–190.

[9] J. Hernandez, M. S. H. Sunny, J. Sanjuan, I. Rulik, M. I. I. Zarif, S. I. Ahamed, H. U. Ahmed, and M. H. Rahman, "Current designs of robotic arm grippers: A comprehensive systematic review," *Robotics*, vol. 12, no. 1, p. 5, 2023.

[10] J. Pledger and M. Wang, "Design and analysis of an end effector using the fin ray structure for integrated limb mechanisms," in *Annual Conference Towards Autonomous Robotic Systems*. Springer, 2022, pp. 40–49.

[11] G. L. Srinivas, A. Javed, and L. M. Faller, "Versatile 3d-printed fin-ray effect soft robotic fingers: lightweight optimization and performance analysis," *Journal of the Brazilian Society of Mechanical Sciences and Engineering*, vol. 46, no. 6, pp. 1–16, 2024.

[12] M. Spenko, "Making contact: A review of robotic attachment mechanisms for extraterrestrial applications," *Advanced Intelligent Systems*, vol. 5, no. 3, p. 2100063, 2023.

[13] A. Parness, M. Frost, N. Thatte, J. P. King, K. Witkoe, M. Nevarez, M. Garrett, H. Aghazarian, and B. Kennedy, "Gravity-independent rock-climbing robot and a sample acquisition tool with microspine grippers," *Journal of Field Robotics*, vol. 30, no. 6, pp. 897–915, 2013.

[14] S. B. Backus, R. Onishi, A. Bocklund, A. Berg, E. D. Contreras, and A. Parness, "Design and testing of the jpl-nautilus gripper for deep-ocean geological sampling," *Journal of Field Robotics*, vol. 37, no. 6, pp. 972–986, 2020.

[15] X. Li, K. Wang, C. Zhao, and H. Zhao, "Design and simulation of an adaptive underactuated gripper for grasping lunar rock," in *2022 International Conference on Service Robotics (ICoSR)*. IEEE, 2022, pp. 38–43.

[16] G. Gorjup, G. Gao, A. Dwivedi, and M. Liarokapis, "A flexible robotic assembly system combining cad based localization, compliance control, and a multi-modal gripper," *IEEE Robotics and Automation Letters*, vol. 6, no. 4, pp. 8639–8646, 2021.

[17] ROBOTIS, *XM430-W350 e-Manual*, ROBOTIS, 2024, accessed: 2024-10-10. [Online]. Available: https://emanual.robotis.com/docs/en/dxl/x/xm430-w350/

[18] Y. Kanbur and U. Tayfun, "Investigating mechanical, thermal, and flammability properties of thermoplastic polyurethane/carbon nanotube composites," *Journal of Thermoplastic Composite Materials*, vol. 31, no. 12, pp. 1661–1675, 2018.

[19] NASA, "Mars facts," NASA, 2024. [Online]. Available: https://science.nasa.gov/mars/facts/

[20] S. Gangatirkar, "Under pressure? here's why you need to check the glass transition temperature of your seal's material," Greene Tweed, 2021. [Online]. Available: https://www.gtweed.com/insights/under-pressure-heres-why-you-need-to-check-the-glass-transition-temperature-of-your-seals-material/

[21] J. O'Connell, "Glass transition temperatures of pla, petg & abs," All3DP, 2024. [Online]. Available: https://all3dp.com/2/pla-petg-glass-transition-temperature-3d-printing/

[22] M. Freiberger, "Polar coordinates," NRICH, University of Cambridge, 2018, accessed: 2024-10-10. [Online]. Available: https://nrich.maths.org/articles/polar-coordinates

[23] D. Cardin-Catalan, S. Ceppetelli, A. P. del Pobil, and A. Morales, "Design and analysis of a variable-stiffness robotic gripper," *Alexandria Engineering Journal*, vol. 61, no. 2, pp. 1235–1248, 2022. [Online]. Available: https://www.sciencedirect.com/science/article/pii/S1110016821004075

[24] J. Falco, K. Wyk, R. Norcross, and E. Messina, "Performance metrics and benchmarks to advance the state of robotic grasping," *National Institute of Standards and Technology (NIST), Gaithersburg, MD, accessed Jan*, vol. 29, p. 2018, 2013.

[25] Y. Hao, Z. Wang, Y. Zhou, W. Zhou, T. Cai, J. Zhang, and F. Sun, "A soft enveloping gripper with enhanced grasping ability via morphological adaptability," *Advanced Intelligent Systems*, vol. 5, no. 6, p. 2200456, 2023.

[26] ROBOTIS, "Dynamixel2arduino: Velocity mode example," https://github.com/ROBOTIS-GIT/Dynamixel2Arduino, 2024. [Online]. Available: https://github.com/ROBOTIS-GIT/Dynamixel2Arduino/blob/master/examples/basic/velocity_mode/velocity_mode.ino

Appendix A Software Design

Program A1 Experimental Test Program for End Effector Validation

```
// Test program written in C for experimental validation of the rock sampling end effector
 // Written by Sophia Schulz, adapted from the Dynamixel2Arduino velocity_mode.ino sketch file (found at https://github.com/ROBOTIS-GIT/Dynamixel2Arduino/blob/master/examples/basic/velocity_mode/velocity_mode.ino)

#include <Dynamixel2Arduino.h>

// Please modify it to suit your hardware.
#if defined(ARDUINO_AVR_UNO) || defined(ARDUINO_AVR_MEGA2560) // When using DynamixelShield
  #include <SoftwareSerial.h>
  SoftwareSerial soft_serial(7, 8); // DYNAMIXELShield UART RX/TX
  #define DXL_SERIAL   Serial
  #define DEBUG_SERIAL soft_serial
  const int DXL_DIR_PIN = 2; // DYNAMIXEL Shield DIR PIN
#elif defined(ARDUINO_SAM_DUE) // When using DynamixelShield
  #define DXL_SERIAL   Serial
  #define DEBUG_SERIAL SerialUSB
  const int DXL_DIR_PIN = 2; // DYNAMIXEL Shield DIR PIN
#elif defined(ARDUINO_SAM_ZERO) // When using DynamixelShield
  #define DXL_SERIAL   Serial1
  #define DEBUG_SERIAL SerialUSB
  const int DXL_DIR_PIN = 2; // DYNAMIXEL Shield DIR PIN
#elif defined(ARDUINO_OpenCM904) // When using official ROBOTIS board with DXL circuit.
  #define DXL_SERIAL   Serial3 //OpenCM9.04 EXP Board's DXL port Serial. (Serial1 for the DXL port on the OpenCM 9.04 board)
  #define DEBUG_SERIAL Serial
  const int DXL_DIR_PIN = 22; //OpenCM9.04 EXP Board's DIR PIN. (28 for the DXL port on the OpenCM 9.04 board)
#elif defined(ARDUINO_OpenCR) // When using official ROBOTIS board with DXL circuit.
  // For OpenCR, there is a DXL Power Enable pin, so you must initialize and control it.
  // Reference link : https://github.com/ROBOTIS-GIT/OpenCR/blob/master/arduino/opencr_arduino/opencr/libraries/DynamixelSDK/src/dynamixel_sdk/port_handler_arduino.cpp#L78
  #define DXL_SERIAL   Serial3
  #define DEBUG_SERIAL Serial
  const int DXL_DIR_PIN = 84; // OpenCR Board's DIR PIN.
#elif defined(ARDUINO_OpenRB)  // When using OpenRB-150
  //OpenRB does not require the DIR control pin.
  #define DXL_SERIAL Serial1
  #define DEBUG_SERIAL Serial
  const int DXL_DIR_PIN = -1;
#else // Other boards when using DynamixelShield
  #define DXL_SERIAL   Serial1
  #define DEBUG_SERIAL Serial
  const int DXL_DIR_PIN = 2; // DYNAMIXEL Shield DIR PIN
#endif

const uint8_t DXL_SPIRAL_ID = 6;
const uint8_t DXL_LINEAR_ID = 3;
const float DXL_PROTOCOL_VERSION = 2.0;
```

```
45
46 #define SCOOP 0
47 #define LIFT 1
48 #define STOP 2
49 int currentState = SCOOP;
50 int lift_start = 0;
51 float spiral_vel = 0;
52 float linear_vel = 0;
53 unsigned long scoop_zero_rpm_start = 0; // Variable to store when 0 RPM
       starts
54 const unsigned long scoop_hold_time = 5000; // Time to hold in SCOOP
       state at 0 RPM (in milliseconds)
55 bool rpm_stable = false; // Flag to check if RPM has been stable for the
       hold time
56
57 Dynamixel2Arduino dxl(DXL_SERIAL, DXL_DIR_PIN);
58
59 //This namespace is required to use Control table item names
60 using namespace ControlTableItem;
61
62 void setup() {
63   // put your setup code here, to run once:
64
65   // Use UART port of DYNAMIXEL Shield to debug.
66   DEBUG_SERIAL.begin(115200);
67
68   // Set Port baudrate to 57600bps. This has to match with DYNAMIXEL
       baudrate.
69   dxl.begin(57600);
70   // Set Port Protocol Version. This has to match with DYNAMIXEL
       protocol version.
71   dxl.setPortProtocolVersion(DXL_PROTOCOL_VERSION);
72   dxl.setPortProtocolVersion(DXL_PROTOCOL_VERSION);
73   // Get DYNAMIXEL information
74   dxl.ping(DXL_SPIRAL_ID);
75   dxl.ping(DXL_LINEAR_ID);
76
77   // Turn off torque when configuring items in EEPROM area
78   dxl.torqueOff(DXL_SPIRAL_ID);
79   dxl.torqueOff(DXL_LINEAR_ID);
80   dxl.setOperatingMode(DXL_SPIRAL_ID, OP_VELOCITY);
81   dxl.setOperatingMode(DXL_LINEAR_ID, OP_VELOCITY);
82   dxl.torqueOn(DXL_SPIRAL_ID);
83   dxl.torqueOn(DXL_LINEAR_ID);
84 }
85
86 void loop() {
87   float current_spiral_velocity = dxl.getPresentVelocity(DXL_SPIRAL_ID,
       UNIT_RPM);
88
89   // Check if we are in SCOOP and if velocity is near 0 RPM
90   if ((currentState == SCOOP) && (millis() > 3000)) { // don't count
       initial motor startup
91     if (current_spiral_velocity < 1.0) {
92       // Start timer if it's not already started
93       if (scoop_zero_rpm_start == 0) {
94         scoop_zero_rpm_start = millis();
95       }
96
```

```
97        // Check if RPM has stayed below the threshold for the required
              time
98        if (millis() - scoop_zero_rpm_start >= scoop_hold_time) {
99          rpm_stable = true;
100       }
101     } else {
102       // Reset timer if RPM goes above threshold during hold time
103       scoop_zero_rpm_start = 0;
104       rpm_stable = false;
105     }
106
107     // Only transition to LIFT if RPM was stable for the whole time
108     if (rpm_stable) {
109       currentState = LIFT;
110       lift_start = millis();
111       scoop_zero_rpm_start = 0; // Reset for next cycle
112       rpm_stable = false;
113     }
114   }
115   else if ((millis() - lift_start) >= 12000 && currentState == LIFT) {
116     currentState = STOP;
117   }
118
119   switch(currentState) {
120     case SCOOP:
121       spiral_vel = -30.0;
122       linear_vel = 1.8;
123       break;
124
125     case LIFT:
126       spiral_vel = 0.0;
127       linear_vel = -1.8;
128       break;
129
130     case STOP:
131       spiral_vel = 0.0;
132       linear_vel = 0.0;
133       break;
134   }
135
136   dxl.setGoalVelocity(DXL_SPIRAL_ID, spiral_vel, UNIT_RPM);
137     // + = open
138     // - = close
139   dxl.setGoalVelocity(DXL_LINEAR_ID, linear_vel, UNIT_RPM); // must be
          0.06 * spiral_vel
140     // ccw (- rpm) = up
141     // cw (+ rpm) = down
142   delay(50);
143 }
```